

https://doi.org/10.1070/QEL17492

Interaction of laser radiation and complexes of gold nanoparticles linked with proteins

S.V. Zar'kov, Yu.A. Avetisyan, A.N. Yakunin, I.G. Meerovich, D. Fixler, A.P. Savitsky, V.V. Tuchin

Abstract. **The results of numerical simulation of the near-field distribution inside and in the vicinity of two types of gold nanoparticles (nanospheres and nanorods) intended for producing complexes of gold nanoparticles linked with proteins and exciting photosensitizers in the wavelength range of 532–770 nm are presented. Quantitative estimates of the field localisation (enhancement) are obtained depending on the type of gold nanoparticles and dimensional factors. The tendency of the red shift of the wavelength at which the maximum local field enhancement is achieved relative to the positions of the maxima of the absorption and scattering cross sections of nanoparticles and complexes is described.**

Keywords: *laser radiation, gold nanoparticles, field localisation, nanoparticle-protein complex, biosensor, protein fluorescence.*

1. Introduction

Despite the rapid development of medical science, diagnostic and therapeutic technologies, including personalised medicine, the diagnosis and treatment of life-threatening diseases is still fraught with many difficulties. For example, due to similar symptoms, low sensitivity and reproducibility of the results of biochemical tests and non-invasive methods of instrumental diagnostics, such as ultrasound, it can be difficult to differentiate between benign and malignant tumour diseases. Alternative methods may be either overly invasive (biopsy) or difficult to access (positron emission tomography, etc.). In this regard, it seems relevant to develop multimodal optical sensors that allow assessing the biochemical parameters of the target organ or tissue for more reliable identification of pathologies at the molecular level. In this case, one of the modalities of such sensors can be used to trigger a therapeutic effect, for example, photothermal, photodynamic, etc., which implements the concept of theranostics.

S.V. Zar'kov, Yu.A. Avetisyan, A.N. Yakunin Institute of Precision Mechanics and Control, Russian Academy of Sciences, ul. Rabochaya 24, 410028 Saratov, Russia; e-mail: anyakunin@mail.ru;
I.G. Meerovich, A.P. Savitsky Bach Institute of Biochemistry, Federal Research Centre 'Fundamentals of Biotechnology' of the Russian Academy of Sciences, Leninsky prosp. 33, stroenie 2, 119071 Moscow, Russia; apsavitsky@inbi.ras.ru;
D. Fixler Institute for Nanotechnology and Advanced Materials BarIlan University, Ramat-Gan, 5290002 Israel;
V.V. Tuchin Saratov State University, ul. Astrakhanskaya 83, 410012 Saratov, Russia; National Research Tomsk State University, prosp. Lenina 36, 634050 Tomsk, Russia; Institute of Precision Mechanics and Control, Russian Academy of Sciences, ul. Rabochaya 24, 410028 Saratov, Russia; e-mail: tuchinvv@mail.ru

Received 24 November 2020
Kvantovaya Elektronika **51** (1) 52–63 (2021)
Translated by V.L. Derbov

It is expected that gold nanoparticles and proteins fluorescent in the red and far red regions will expand the range of applications of fluorescent proteins and sensors based on two fluorescent proteins separated by a proteolytic enzyme recognition site for biomedical purposes. Such nanohybrids, equipped with additional modalities (for example, a pH sensor based on known fluorescent dyes), can operate *in vivo* as biological computing devices and independently detect anomalies, and, keeping in mind the possibility of using gold nanoparticles (GNPs) in anticancer therapy [1], subsequently trigger the therapeutic process.

GNPs with various coatings and ligands at present are widely used for biological and biomedical purposes *in vitro* and *in vivo* due to their photophysical properties. GNPs can be used as contrast agents for many optical imaging methods, as well as for photothermal destruction of tumour cells and microorganisms [2–7].

For a long time, GNPs were considered a material largely inert biologically in relation to a living cell and living organism in general. However, the studies of recent decades on the use of GNPs as agents for nanodiagnostics and nanomedicine [8, 9] provide a wealth of information about the biodistribution, pharmacokinetics, and potential toxicity of gold nanopreparations [10–12]. In particular, as shown in [13], *in vitro* cytotoxicity of gold nanoparticles with a concentration not exceeding 10^{12} nanoparticles ml^{-1} is not observed for nanoparticles 3–100 nm in size. The data on the *in vivo* toxicity of GNP are rather ambiguous. Studies show that the main targets for the accumulation of GNPs with a size of 10–100 nm in a living organism are the organs of the reticuloendothelial system. The peculiarities of GNP accumulation in the liver and lymphoid tissue should be taken into account when using them *in vivo* in order to avoid provoking inflammatory processes.

The authors of [13] also draw attention to the fact that the effect of GNP penetration through the blood-brain barrier critically depends on the size of nanoparticles, the upper limit of which is about 20 nm. GNPs with a diameter of 1–2 nm can potentially be more toxic due to the possibility of irreversible binding to key cell biomolecules (for example, DNA) and subsequent influence on the functioning of cellular molecular processes.

From the point of view of toxicity, the properties of the modified GNP surface are also important. For example, when GNPs are conjugated with polyethylene glycol (PEG), their *in vitro* stability is significantly improved, preventing salt aggregation. The bioavailability and stability of nanoparticles *in vivo* increase, which leads to an increase in the time of their circulation in the bloodstream. *In vivo*, PEGylated nanoparticles preferentially accumulate in tumour tissue due to increased permeability of tumour vessels and are retained in it

due to reduced lymph drainage. In addition, PEGylated nanoparticles are less available to the immune system [2].

The size of nanoparticles for *in vivo* use should also be determined by the purpose of theranostics. In this case, it is necessary to take into account both the possibility of filtering nanoparticles by the kidneys for excretion from the body, and the possibility of these nanoparticles passing through the vascular network (in particular, for delivery to the tumour) [14].

The final coating of nanoparticles is determined by the requirements for the biocompatibility, bioavailability and biodistribution of GNPs in cells *in vitro* and in a living organism, as well as their aggregation and chemical resistance in various biological microenvironments. In addition, it is possible to supply nanoparticles with receptor-specific molecules. The choice of nanoparticles is dictated by requirements for the chemical and physical properties of modified nanoparticles: size, chemical composition, surface functionality, fluorescence quantum yield, fluorescence peak width, fluorescence maximum wavelength, chemical stability, and photostability.

Gold nanoparticles can serve as vehicles for a kind of logic gates, allowing the use of several detection methods and at the same time serving as platforms for potentially complex structures [15–17]. GNPs are well known for their biocompatibility [18, 19], the ability to modify the surface and interact with nearby fluorescent materials [20].

With the development of nanotechnology, it became possible to adapt nanoparticles for conjugation with environmentally responsive and activated probes that can only respond to certain biological stimuli, enzymes, or microenvironmental parameters [21]. Subsequently, the combination of a number of biological triggers can also be considered as a form of biological computers [22].

GNP suspensions can be obtained by the known method of citrate reduction of chloroauric acid (Turkevich method) [23]. Gold nanospheres of various diameters with a narrow size distribution are prepared by nucleation in a medium containing micelles of cetyltrimethylammonium chloride and ascorbic acid as a reducing agent [24], and gold nanorods are prepared by a seed-mediated method based on 'soft' matrices, which also uses surfactants (cetyltrimethylammonium bromide) to form soft matrices and ascorbic acid as a reducing agent [25].

There are many methods for modifying GNPs with proteins [26]. The attachment of streptavidin to GNPs can occur through its direct adsorption on uncoated nanoparticles [27]. Covalent conjugates of GNPs (nanospheres, nanorods) can be produced by the following methods:

– attachment of streptavidin to activated groups (for example, carboxyl) on the GNP surface [28];

– attachment of streptavidin, previously modified with active groups, to GNPs [29]; and

– finally, covalent conjugates of proteins (in particular, streptavidin) with GNPs (nanospheres, nanorods) can be obtained by covalently attaching the protein to nanoparticles previously coated with activated PEG, for example, methoxy-PEG (85%) and carboxylated PEG (15%) [30].

The relatively high transparency of tissues in the far red and near IR regions of the spectrum allows wide use of a number of fluorescent proteins in biomedical studies [31–33] with nonradiative (Förster) resonant energy transfer. The maximum of the absorption spectrum of some of them is located not only in the visible part of the wavelength range, but also in the near-IR range [34]. The synthesis of nanoparticle–protein complexes [31, 32] promises a significant increase in the efficiency of biomedical applications of fluorescent proteins due to the effects of enhancement of the laser radiation field on plasmonic nanoparticles.

In this regard, the main aim of this work was to construct a model and to theoretically study the features of the formation of localisation zones of the near field in the vicinity of GNP, since the intensity of this field determines the efficiency of exciting photosensitizer molecules [35] under laser irradiation. Quantitative assessments were made of the effect of the optical properties and geometric parameters of the multilayer structure of a sandwich photosensitizer on the spectral and fluorescent properties of nanoparticle–protein complexes.

2. Statement of the problem

In view of the potential choice of fluorescent proteins with an absorption spectrum in a wide wavelength range, we will consider two types of GNPs, i.e. gold nanospheres and gold nanorods. This will ensure the study of the plasmon-resonance enhancement of the local field both in the green region (λ = 532 nm) near nanospheres and at the red edge of the wavelength range (λ = 630 and 730 nm), up to the near-IR range (λ = 770 nm), near nanorods. For nanoparticles made of a material with specified optical characteristics, tuning of the plasmon resonance to the specified wavelengths is possible by varying the dimensional parameters of these nanoparticles. For nanospheres, this parameter is the radius R. For nanorods (which are modelled by straight circular cylinders of height L and diameter d with two hemispheres of the same diameter d at their ends) these parameters are the volume V and aspect ratio AR of the nanorod length h (taking into account the cylindrical part and rounded ends) to the cross-section diameter d: AR = h/d. The general regularities of changes in the dependences of the spectral characteristics of gold nanorods on their sizes have been thoroughly investigated both theoretically and experimentally, e.g., in [36, 37]. Therefore, taking into account the known experience, the tuning of gold nanorods to resonance wavelengths λ = 630, 730, and 770 nm will be carried out, for definiteness, at AR = 2, 2.5, and 3, respectively.

The requirements for the synthesis of the dimensional parameters of GNPs with predetermined plasmon resonance wavelengths will be formulated based on the analysis of the results of finite element modelling of the spectral properties of GNPs using the Comsol Multiphysics commercial software package (Wave Optics module). In the simulation, it was assumed that the nanoparticle is immersed in an aqueous medium and is irradiated by a plane linearly polarised electromagnetic wave. To describe the bulk dielectric functions of gold and water, we used the interpolation of the data from [38, 39].

It is known that for plasmonic nanoparticles of arbitrary shape, the size of which is comparable to the electron mean free path l_e in a bulk metal, the dielectric function cannot be correctly described by the dielectric function of the bulk metal [34]. Instead, the dielectric function of a particle can be represented as

$$\varepsilon_{\mathrm{Au}}(\omega, a) = \begin{cases} \varepsilon_{\mathrm{Au\,bulk}}(\omega), & a \gg l_e, \\ \varepsilon_{\mathrm{Au\,bulk}}(\omega) + \Delta\varepsilon(\omega, a), & a \approx l_e, \end{cases} \quad (1)$$

where $\varepsilon_{\mathrm{Au}}(\omega, a)$ is the dielectric function of a GNP of size a; $\varepsilon_{\mathrm{Au\,bulk}}(\omega)$ is the dielectric function of bulk gold; and $\Delta\varepsilon(\omega, a)$

is a correction that takes into account the contribution of the size-dependent electron scattering to the Drude part of the dielectric function in accordance with the formula

$$\Delta\varepsilon(\omega, L_{\text{eff}}) = \frac{\omega_p^2}{\omega^2 + i\omega\gamma_b} - \frac{\omega_p^2}{\omega^2 + i\omega(\gamma_b + A\hbar v_F/L_{\text{eff}})}, \quad (2)$$

where $\omega_p = 9$ eV is the plasma frequency; $\gamma_b = 0.09$ eV is the damping constant for bulk gold; A is the electron scattering constant (assumed equal to 0.7 for a sphere [40] and 0.46 for nanorods) [41]; $v_F = 1.4 \times 10^{15}$ nm s^{-1} is the Fermi velocity; and L_{eff} is the effective mean free path of an electron. For a sphere, scattering was assumed to be diffuse, i.e., $L_{\text{eff}} = 4R/3$; for nanorods, the Schatz–Coronado formula [42] was used to obtain $L_{\text{eff}} = AR^{-1}(h - d/3)$.

At the second stage of the study, a comparative analysis of the features of the distribution of the electric field strength enhancement factor near GNP will be carried out, according to the results of which it will be possible to judge the acceptability of using the investigated nanoparticles for the synthesis of effective nanoparticle–protein complexes.

The final stage of the study is devoted to the construction of a phenomenological model of a sandwich complex with distributed parameters and an assessment of the effect of the protein layer on the spectral properties and parameters of the electric field localisation, which determine the protein fluorescence.

3. Numerical modelling and discussion of results

3.1. Tuning the GNP plasmon resonance

The procedure for tuning the plasmon resonance in nanoparticles consists in determining their dimensional parameters to ensure plasmon resonance at specified wavelengths. The choice of parameters is based on the analysis of the results of parametric calculation of the absorption and scattering spectra of nanoparticles. In this case, the variable parameters are the radius R (for nanospheres) and the dimensions h and d at a given aspect ratio AR (for nanorods). Generally, a nanosphere can be formally considered a nanorod with AR = 1. This allows unifying the approaches to modelling nanoparticles of both types, although some differences remain. In particular, the effects of absorption and scattering of a plane linearly polarised wave by a nanorod substantially depend on its orientation with respect to the field polarisation vector, whereas the process of interaction of such a wave with a nanosphere is polarisation-independent.

The results of parametric modelling of the spectral dependences of the absorption cross section C_{abs} and the scattering cross section C_{sca} for nanospheres (AR = 1) are shown in Figs 1a and 1b. It can be seen that the curves for C_{abs} and C_{sca} increase monotonically with increasing radius of nanospheres. At the same time, there is an insignificant red shift of their

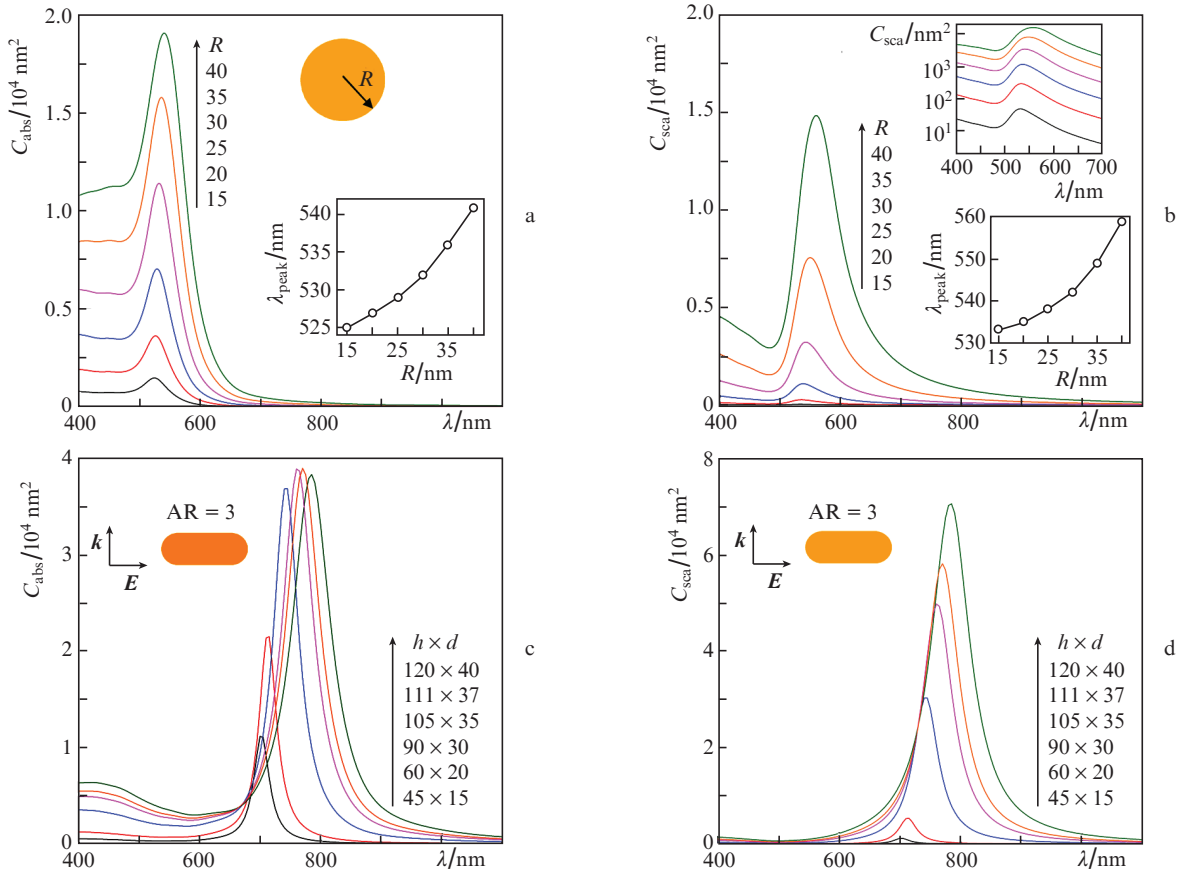

Figure 1. (Colour online) Spectra of (a, c) absorption and (b, d) scattering cross sections for nanospheres of different radii (shown in nm in Figs 1a and 1b) and nanorods of various sizes $h \times d$ (shown in nm in Figs 1c and 1d) with AR = 3. The lower insets in Fig 1a and 1b show the dependences of the plasmon resonance wavelength λ_{peak} on the nanosphere radius. The upper inset in Fig. 1b shows the spectrum of the scattering cross section C_{sca} on a logarithmic scale in the wavelength range 400–700 nm. The orientation of the wave vector $\boldsymbol{k}$ and field strength $\boldsymbol{E}$ relative to the nanorod is shown in the corresponding figures.

maximum. The position of the maxima of the scattering cross section is also characterised by a certain red shift in comparison with the position of the maxima of the absorption cross section for nanospheres of the same size; the maximum shift of the maximum when changing the radius of nanospheres in the studied size range reaches 15 nm.

The results of parametric modelling of the spectral dependences of the absorption cross section C_{abs} and the scattering cross section C_{sca} for nanorods (using the example of nanorods with AR = 3), shown in Figs 1c and 1d, indicate the existence of other trends. First, quantitatively, the red shift of the extrema of both absorption and scattering with increasing nanorod sizes is more significant. The change in the resonance wavelength is 3% for nanospheres, and in the case of nanorods, it reaches almost 20%. Second, the resonance absorption cross section does not grow monotonically with increasing nanorod sizes, but has a local extremum near $\lambda = 770$ nm, as follows from the analysis of the data in Fig. 1c.

For easier perception of the spectral features of the dependences of the absorption, C_{abs}, and scattering, C_{sca}, cross section, the information about the extrema of the obtained spectra is presented in Fig. 2 (nanospheres with AR = 1) and Fig.3 (nanorods with AR = 3) in the form of dependences of these cross sections on the nanoparticle volume V. Introducing a generalised variable V makes it possible to compare different types of nanoparticles in a single coordinate system. The calculated points on the curves plotted when moving from left to right correspond to the sizes of nanospheres and nanorods indicated in Fig. 1, in order of increasing sizes. From Fig. 2a, it can be found that the desired resonant wavelength λ =

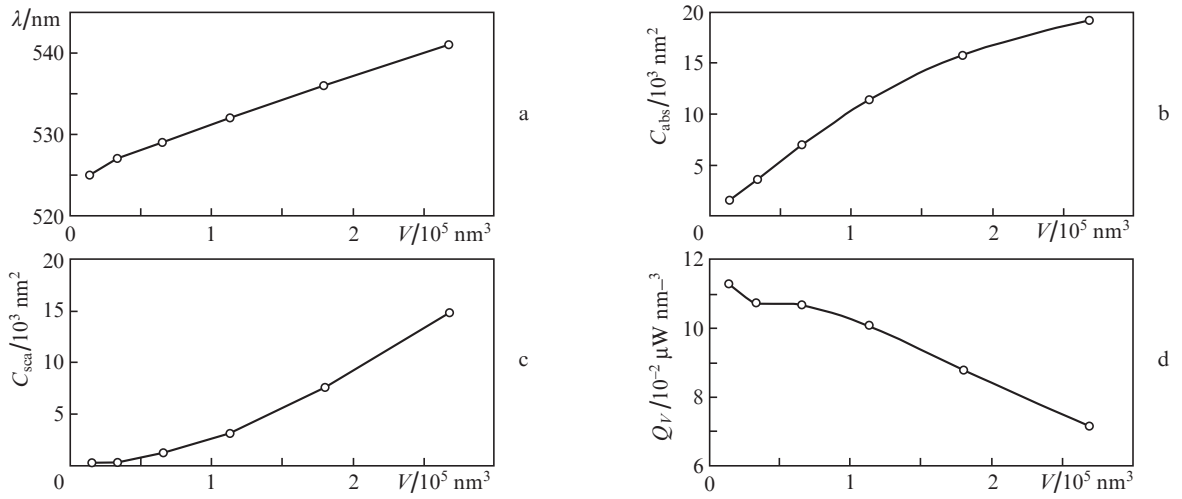

Figure 2. Dependences of the plasmon resonance wavelength (a), the absorption (b) and scattering (c) cross sections at the plasmon resonance wavelength, as well as the specific volume absorption power of a nanoparticle irradiated with a beam with an intensity of 1 μW nm^{-2} at the wavelength of the plasmon resonance (d) on the volume V of nanospheres (AR = 1).

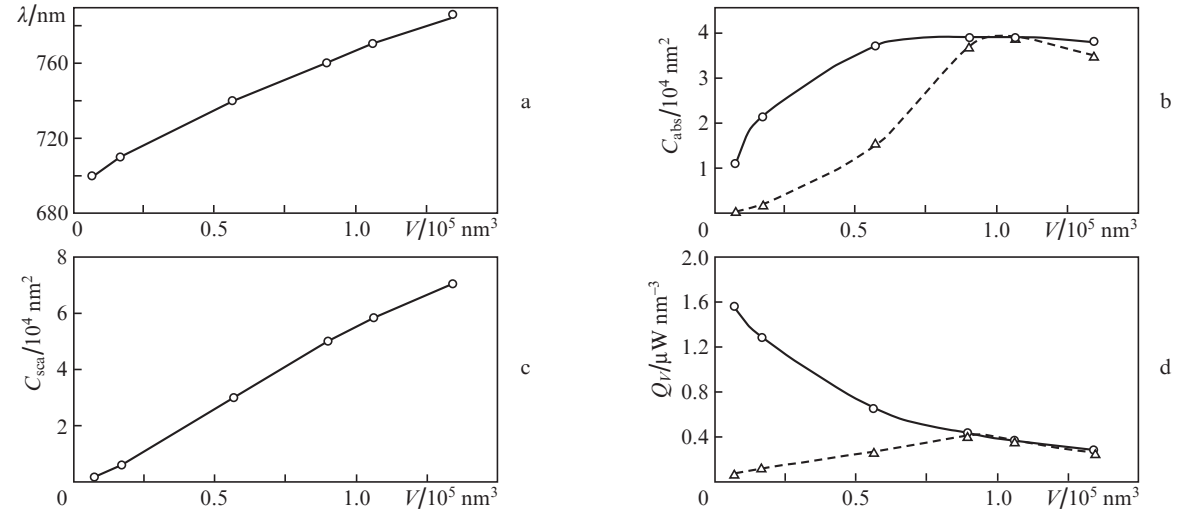

Figure 3. Dependences of the plasmon resonance wavelength (a), the absorption cross section at the plasmon resonance wavelength and at the operating wavelength $\lambda = 770$ nm (b), the scattering cross section at the plasmon resonance wavelength (c), and the specific volume absorption power of a nanoparticle irradiated with a beam with an intensity of 1 μW nm^{-2} at the wavelength of the plasmon resonance and at λ= 770 nm (d) on the volume V of nanorods with AR = 3; the circles correspond to the calculated data obtained at the plasmon resonance wavelength, and the triangles at $\lambda = 770$ nm.

532 nm is inherent in a nanosphere with a radius of $R = 30$ nm, and Fig. 3b shows that the resonant wavelength of $\lambda = 770$ nm is inherent in a nanorod with parameters $h = 111$ nm and $d = 37$ nm. Similar simulation results for nanorods with AR = 2 and 2.5 made it possible to establish that the plasmon resonance wavelength $\lambda = 630$ nm is provided in nanorods with dimensions $h = 80$ nm and $d = 40$ nm, and $\lambda = 730$ nm – in nanorods with dimensions $h = 115$ nm and $d = 46$ nm.

Additional information about the specific absorption power Q_V by nanoparticles, presented in Figs 2d and 3d, makes it possible to estimate the possible thermal effect of laser radiation on the nanoparticle and the surrounding biological tissue. Note that, upon irradiation of nanorods and nanospheres with a laser beam of the same intensity, the Q_V values for nanorods are at least five times higher than Q_V for nanospheres. Since with the accepted range of variation of the sizes (volume) of nanospheres, the plasmon resonance wavelength changes by no more than 3%, the effect of such deviations from the operating wavelength $\lambda = 532$ nm on C_{abs} and C_{sca}, as well as on Q_V, turns out to be negligible. A different situation is observed in the case of nanorods: as follows from Figs 3b and 3d, when the wavelength of the plasmon resonance of the nanorod deviates from the working one ($\lambda = 770$ nm), the values of C_{abs} and Q_V can change significantly (up to 20 times).

3.2. Calculation of the distribution of the enhancement of the local field of a laser beam on a GNP

The problem of studying the regularities of the formation of zones of localisation of the near field in the vicinity of a GNP acquires special significance in the context of the issues considered in this work, since it is exactly the electric field strength that determines the efficiency of excitation of photosensitizer molecules during laser irradiation. Therefore, it is reasonable to introduce the function of spatial coordinates $\xi_{E^2} = |E|^2/|E_0|^2$, where E is the local value of the complex amplitude of the total (resultant) field, and E_0 is the complex amplitude of the irradiating field, modeled by us in the form of a plane electromagnetic wave.

Topograms of the ξ_{E^2} distribution in the $(\boldsymbol{E},\boldsymbol{k})$ plane, where $\boldsymbol{k}$ is the wave vector of the irradiating field inside and outside the four plasmonic nanoparticles defined above, are shown in Fig. 4. The choice of this plane, hereinafter called the plane of incidence, is due to the greatest inhomogeneity of the distribution of ξ_{E^2}, which is explained by the maximum values of the phase incursions of the field in this plane and the existence of a global maximum of ξ_{E^2}. The first colour scales to the right of each topogram indicate the range of variation of ξ_{E^2} inside the nanoparticle, determining the distribution of the specific radiation absorption power Q_V, and the second to the right, the range of variation of this coefficient near the nanoparticle. It can be seen that the vicinity of the hemispherical tip of the nanorods is a zone of pronounced localisation of the electric field with increased strength, in which the probability of initiating fluorescence of protein molecules upon irradiation with a low-intensity optical beam (Figs 4b–4d) is highest. It is characteristic that near the middle part of the nanorods, the near-field enhancement is approximately six to seven times lower. The inhomogeneity of the angular distribution of ξ_{E^2} at the surface of the nanosphere is practically the same. However, from a comparison of the data in Figs 4b–4d with the data in Fig. 4a it follows that in any of the considered cases, ξ_{E^2} for nanorods is no less than that for a nanosphere. At the same time, it is necessary to take into account the absence of the polarisation dependence of local fields upon irradiation of the nanosphere.

For the convenience of a comparative assessment of the optical characteristics of different types of studied nanoparticles with the desired resonance parameters, Fig. 5 shows the results of modelling the spectral dependences of the absorption, scattering, and extinction cross sections, as well as the maximum values of the field enhancement factor ξ_{E^2}.

Figure 6 allows a quantitative estimate of the inhomogeneity of the angular distribution of ξ_{E^2} at the surface and at a certain distance from the surface of nanoparticles, i.e., in a certain zone of distributed localisation of the near field. Generalised data on the field localisation parameters are summarised in Table 1.

It follows from the analysis of the data that gold nanorods have a significant potential and promise for the creation of complexes with the excitation of fluorescent proteins in the near-IR range. This is based on approximately 20 times higher values of the maximum ξ_{E^2} in a given localisation zone compared to the enhancement for nanospheres, as follows from Fig. 5d, and about 300 times higher values of the minimum

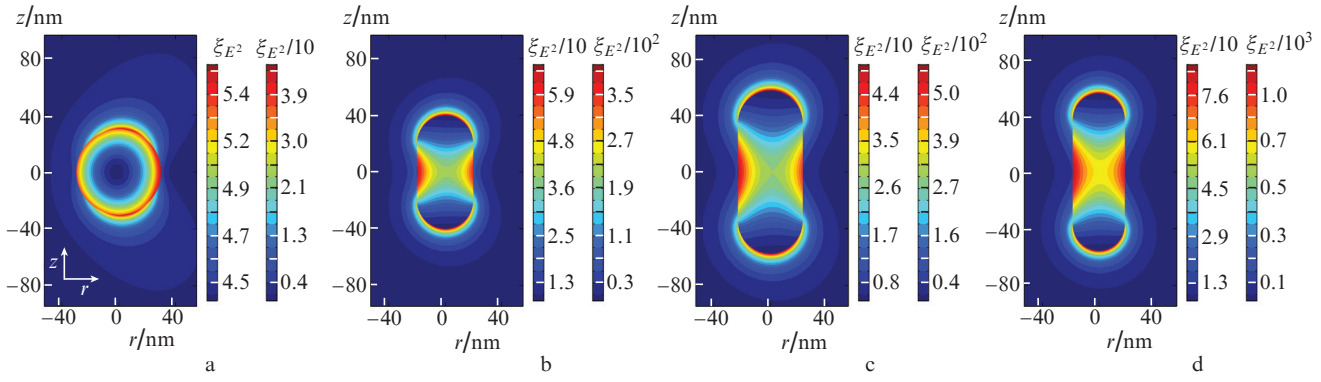

Figure 4. (Colour online) Topograms of the distributions of the field enhancement factor ξ_{E^2} in the central sections of nanoparticles by the $(\boldsymbol{E}, \boldsymbol{k})$ plane. Nanoparticles with sizes $(h \times d)$ and aspect ratios (AR) 60 nm (AR = 1) (a), 80 × 40 nm (AR = 2) (b), 115 × 46 nm (AR = 2.5) (c), 111 × 37 nm (AR = 3) (d) were irradiated at wavelengths $\lambda = 532$, 630, 730, and 770 nm, respectively. The polarisation vector is directed along the z axis.

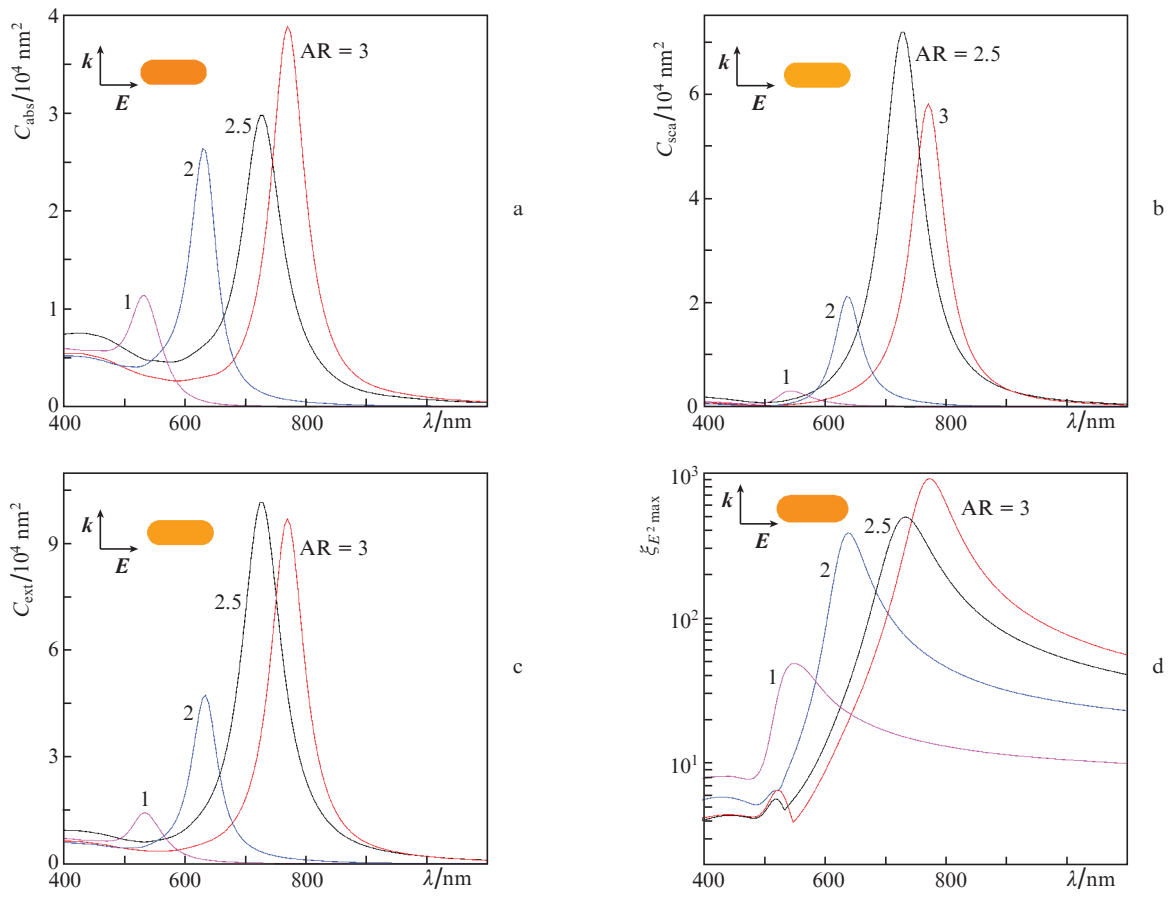

Figure 5. Spectral dependences of (a) absorption, (b) scattering, and (c) extinction cross sections, as well as the maximum value of the electric field enhancement factor (d) for a nanosphere with a radius of $R = 30$ nm (AR = 1) and nanorods with sizes ($h \times d$) 80×40 nm (AR = 2), 115×46 nm (AR = 2.5), 111×37 nm (AR = 3).

Table 1. Field localisation parameters in the vicinity of nanorods.

Characteristics of nanorods	Range of ξ_{E^2} variation in the localisation zone limited by the radial layer thickness Δ			Laser beam intensity I/I_0 ensuring the same minimum strength in the electric field localisation zone at a distance from the surface Δ		
	$\Delta = 5$ nm	$\Delta = 10$ nm	$\Delta = 15$ nm	$\Delta = 5$ nm	$\Delta = 10$ nm	$\Delta = 15$ nm
AR = 1 ($R = 30$ nm)	1.5–37.8	0.4–37.8	0.2–37.8	168	290	300
AR = 2 (80×40 nm)	76–320	32–320	16–320	3.3	3.7	3.7
AR = 2.5 (115×46 nm)	130–475	67–475	37–475	1.9	1.7	1.6
AR = 3 (111×37 nm)	250–870	117–870	60–870	1.0	1.0	1.0

ξ_{E^2} in the same localisation zone (see Table 1, the column for the intensity of the laser beam I/I_0 required to ensure the same minimum intensity in the zone of the electric field localisation at a distance Δ from the nanoparticle surface).

3.3. Phenomenological model of a sandwich structure with distributed parameters

Technologically, the procedure for synthesising a composite structure, in which the conjugation of GNP with the protein coat is provided, is nontrivial and implies the sequential multistage formation of a multilayer system [32, 43]. A schematic representation of the synthesised structure is shown in Fig. 7 on the left. Its main components are GNP itself, a PEG-based spacer, a streptavidin–biotin complex, and TagRFP fluorescent protein molecules. As established in [44, 45], and also as follows from the results of Ref. [46], the thickness of the PEG layer, depending on the mass of PEG molecules used for GNP modification (varying in the range of 2–5 kDa), can be 10 nm or more. The thickness of the streptavidin layer is 5.6 nm, and the TagRFP layer is 4 nm. The existence of a thin binding layer of the tetramethylene group (biotin) less than 0.25 nm thick can be ignored from the point of view of its possible effect on the optical properties of the structure. Taking into account the properties of PEG and streptavidin ($n_1 \approx 1.5$), as well as TagRFP [$n_2 = 1.67 + i\kappa_2(\lambda)$], the phenomenological computational model can be represented as a GNP with a three-layer sandwich structure, as shown in Fig. 7 on the right.

In the calculation, we used the optical parameters of the fluorescent protein TagRFP taken from [43], including the spectrum of the absorption coefficient κ_2 shown in Fig. 8 of

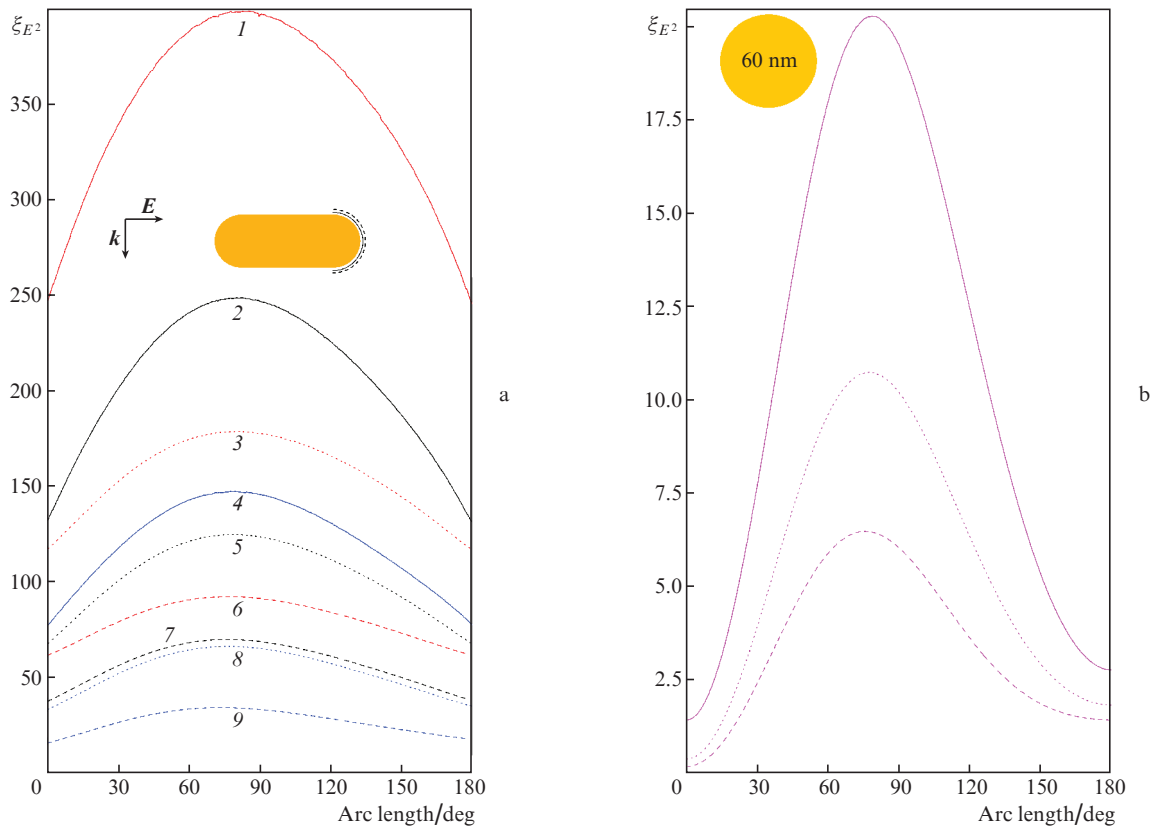

Figure 6. Angular distributions of the enhancement factor ξ_{E^2} in the vicinity of a hemispherical tip of nanorods of three sizes (a) and in the vicinity of a nanosphere 60 nm in diameter (b). Solid curves are distributions obtained at a distance of 5 nm from the surface of nanoparticles, dotted curves are obtained at a distance of 10 nm, and dashed curves at a distance of 15 nm. Dimensions ($h \times d$) and aspect ratios (AR) of nanorods: 111 × 37 nm (AR = 3) for curves *1*, *3*, and *6*; 115 × 46 nm (AR = 2.5) for curves *2*, *5*, and *7*; and 80 × 40 nm (AR = 2) for curves *4*, *8*, and *9*. For nanorods, the calculations were performed at wavelengths λ = 770, 730, and 630 nm, respectively, for a nanosphere, at λ = 532 nm.

Ref. [47]. The extinction coefficient α of the TagRFP fluorescent protein (in cm^{-1}) is found using the formula

$$\alpha = \alpha_m \frac{\rho C}{M}, \tag{3}$$

where α_m is the molar extinction coefficient (in M^{-1} cm^{-1} or mol^{-1} dm^3 cm^{-1}) ; ρ is the density of the substance (in g cm^{-3}); C is the volume concentration of the substance; an M is the molar mass (in kDa). The imaginary part of the refractive index (absorption index) is determined by the expression

$$\kappa_2 = \frac{\lambda}{4\pi}\alpha. \tag{4}$$

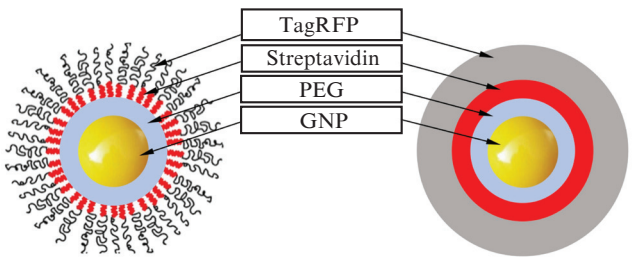

Figure 7. (Colour online) To the definition of a phenomenological sandwich structure with distributed parameters.

3.4. Calculation of the enhancement factor distribution for the local field of the laser beam on the protein–GNP complexes

The effect of the protein coating on the optical properties of the protein–GNP complex was estimated using the mathematical model constructed and described above. Since the absorption maximum of the fluorescent protein TagRFP, as follows from the data shown in Fig. 8, is observed at λ = 555 nm, here the main attention will be paid to modelling complexes based on gold nanospheres. The wavelength of their plasmon resonance, in contrast to the resonance wavelength of nanorods, is the closest to that indicated. The calculated spectral dependences of the optical properties of such a nanosphere with a diameter of 60 nm – gold uncoated and gold with a multilayer coating – are shown in Figs 9a and 9b. For a sphere with a multilayer coating, the following thicknesses of the coating layers were chosen: 15 nm for the first (inner) layer simulating the complex of PEG and streptavidin ($n_1 \approx 1.5$) and 4 nm for the second (outer) layer, for which the optical properties of TagRFP were specified [n_2 = 1.67+ i$\kappa_2(\lambda)$]. A 30% increase in the maximum absorption cross section for a multilayer structure is observed, which can be

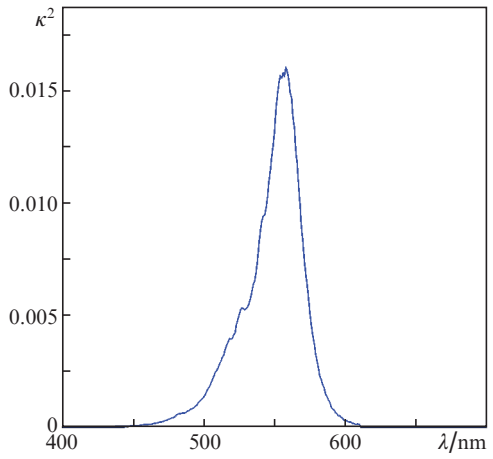

Figure 8. Spectrum of the absorption index κ_2 of the fluorescent protein TagRFP, calculated on the basis of the spectrum of the molar extinction coefficient (in M^{-1} cm^{-1}) [47].

explained by a number of reasons, including additional absorption in the protein layer, the processes of refraction and re-reflection of light in the multilayer structure, and an increase in its total volume (diameter) compared to the size of the gold nanosphere. An increase in the maximum of the scattering cross section is even more significant: it increases by 100% compared to an uncoated nanosphere. An increase in the extinction of conjugates has been described previously, e.g., by the authors of Ref. [48]. The spectral dependence of the maximum enhancement factor $\xi_{E^2\max}$, shown in Fig. 9c, exhibits an opposite tendency. When the protein coating is formed, the maximum enhancement is reduced by 15%. And in the protein layer, the decrease in ξ_{E^2} is greater, which follows from the analysis of the azimuthal distribution in Fig. 9d and is explained by the increased value of the real part of the TagRFP refractive index.

Of particular interest, in our opinion, is the observed tendency of the red shift of the wavelength at which the maximum enhancement factor ξ_{E^2} of the local field is reached, relative to the positions of the maxima of the absorption and scattering cross sections for uncoated gold nanospheres and multilayer structures. The influence of this effect is illustrated by the results of calculations of the radial distributions of ξ_{E^2} performed at two wavelengths of the irradiating laser beam. The first of them (532 nm) corresponds to the plasmon absorption resonance for a gold nanosphere with a diameter of 60 nm without coating (Fig. 10). The second wavelength (555 nm) corresponds to the resonance calculated on the basis of a numerical experiment on tuning the wavelength of the irradiating beam according to the criterion of achieving maximum ξ_{E^2} in a multilayer coated structure.

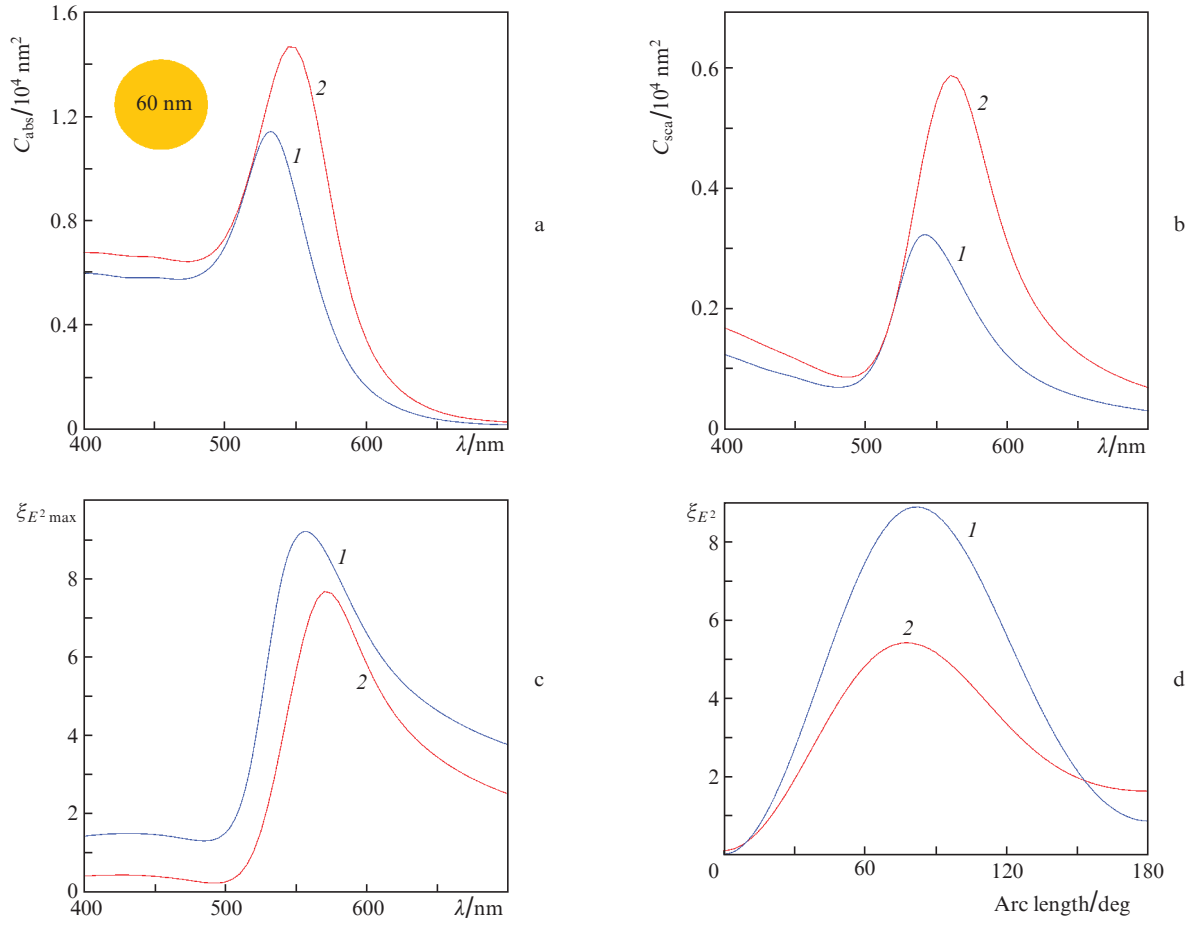

Figure 9. Spectral dependences of the absorption cross section (a), scattering cross section (b) and the maximum value of the field enhancement factor $\xi_{E^2\max}$ (c), as well as the azimuthal distribution of ξ_{E^2} at a distance of 15 nm from the surface of the gold nanosphere (TagRFP fluorescent protein layer) at λ = 532 nm (d) for a gold nanosphere without coating (*1*) and with protein coating (*2*).

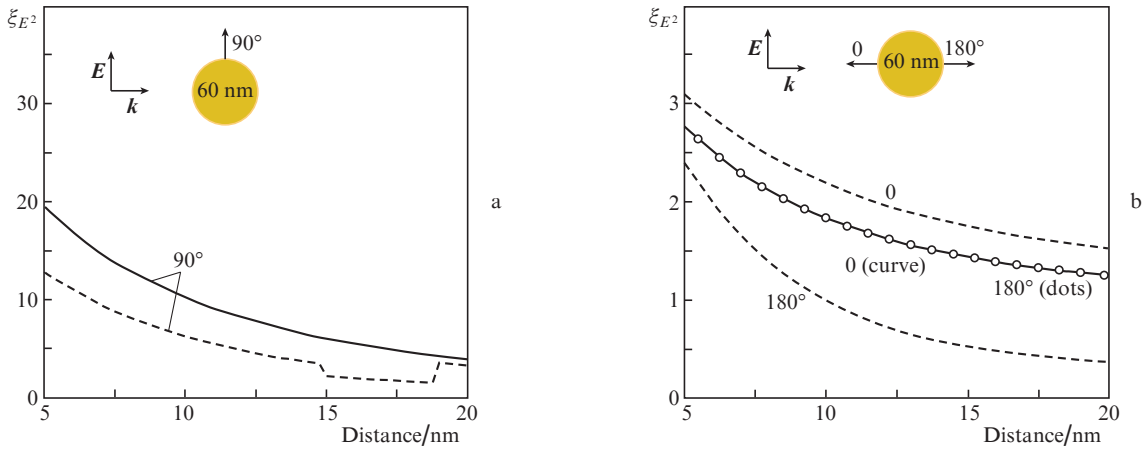

Figure 10. Radial distributions of the enhancement factor ξ_{E^2} at $\lambda = 532$ nm in the vicinity of a gold nanosphere without coating (solid curves) and with a coating (dashed curves) at different directions of the radius vector (indicated in the insets), along which the distributions are plotted.

Comparison of the simulation data shown in Figs 10a and 11a allows a conclusion that the specified adjustment of the wavelength of the irradiating beam significantly reduces the negative effect of the protein coating on the value of the maximum enhancement factor ξ_{E^2} for the structure. By negative effect we mean a decrease in ξ_{E^2} after the formation of a multilayer structure on the gold nanosphere. Whereas in the first case (with irradiation at $\lambda = 532$ nm) the curve for the uncoated nanosphere is located noticeably higher than the corresponding curve for the coated nanosphere, in the second case ($\lambda =$ 555 nm) the difference in the positions of both curves is minimal. The jump with decreasing ξ_{E^2} values with a change in the radial distance from 15 to 19 nm corresponds to the region of the protein layer and is explained by the higher value of the real part of the refractive index n_2. It is exactly this region, which is of primary interest for local field optimisation. An estimate based on the results of the performed simulation indicates that the tuning of the probing signal in the case under consideration provides an increase in the enhancement factor ξ_{E^2} and, consequently, the efficiency of the fluorescence response by a factor of 2.3. Analysis of the results shown in Table 1, as well as in Figs 10 and 11, makes it possible to propose a decrease in the thickness of the inner transition layers of a multilayer structure as an additional possible way to increase the efficiency of the protein coating. When approaching the surface of a gold nanosphere (plasmonic field concentrator), the value of ξ_{E^2} increases nonlinearly, which is convincingly shown there.

The distributions of ξ_{E^2} in two opposite directions parallel (curve) and antiparallel (dots) to the wave vector $\boldsymbol{k}$, shown in Figs 10b and 11b, demonstrate the appearance of significant asymmetry during the formation of a multilayer coating. In the case of uncoated gold nanospheres, both distributions practically coincide.

The degree of influence of the radius of the gold nanosphere on the change in the enhancement factor ξ_{E^2} in the region of the protein layer (it is assumed that the thickness of the multilayer coating remains the same when the size of the nanosphere changes) can be judged from the nomogram shown in Fig. 12. Figure 12a shows a family of spectral dependences of ξ_{E^2} for nanospheres, the radius of which varies in the range of 30–60 nm. It is seen that the extrema of the curves for ξ_{E^2} change nonmonotonically. Their positions in the studied wavelength range also change. The transformation of this family of curves can be assessed by comparing with the results of modelling the spectral dependences of ξ_{E^2} shown in Fig. 12b. The general tendency manifests itself in a decrease in the value of the local maximum of each curve and

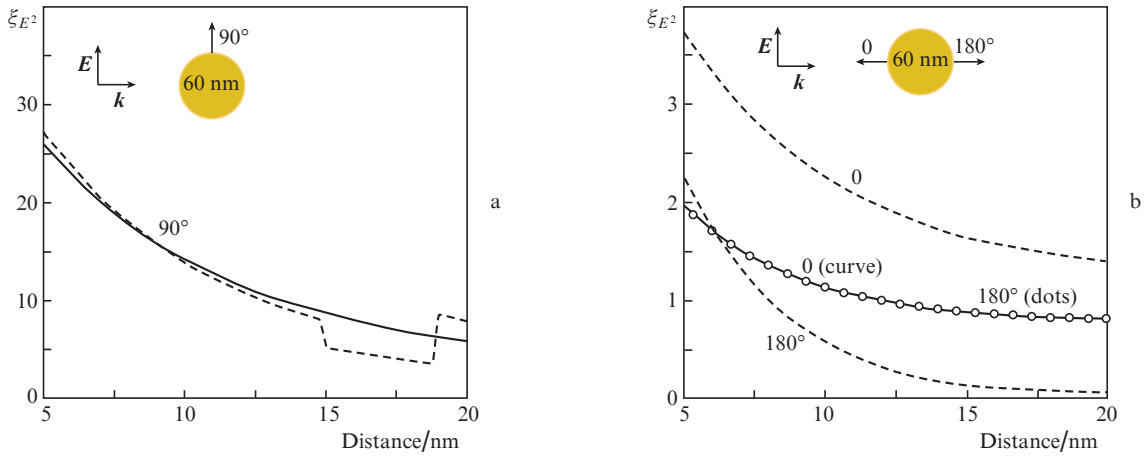

Figure 11. Same as in Fig. 10, but for $\lambda = 555$ nm.

its shift towards long waves. Examples of quantitative and qualitative changes in the $\xi_{E^2}(R)$ dependences upon irradiation of coated and uncoated nanospheres at two different wavelengths are shown in Fig. 12c. It can be seen that R = 40 nm is the optimal nanosphere size for the fabrication of a fluorescent structure, in which it is supposed to excite the protein photosensitizer by radiation at λ = 555 nm. A deviation from this size within the limits indicated in Fig. 12 can lead to a decrease in ξ_{E^2} by almost 1.4 times. When irradiated with a laser beam at a wavelength λ = 532 nm, the factor ξ_{E^2} decreases by a factor of two and weakly depends on the size of nanoparticles.

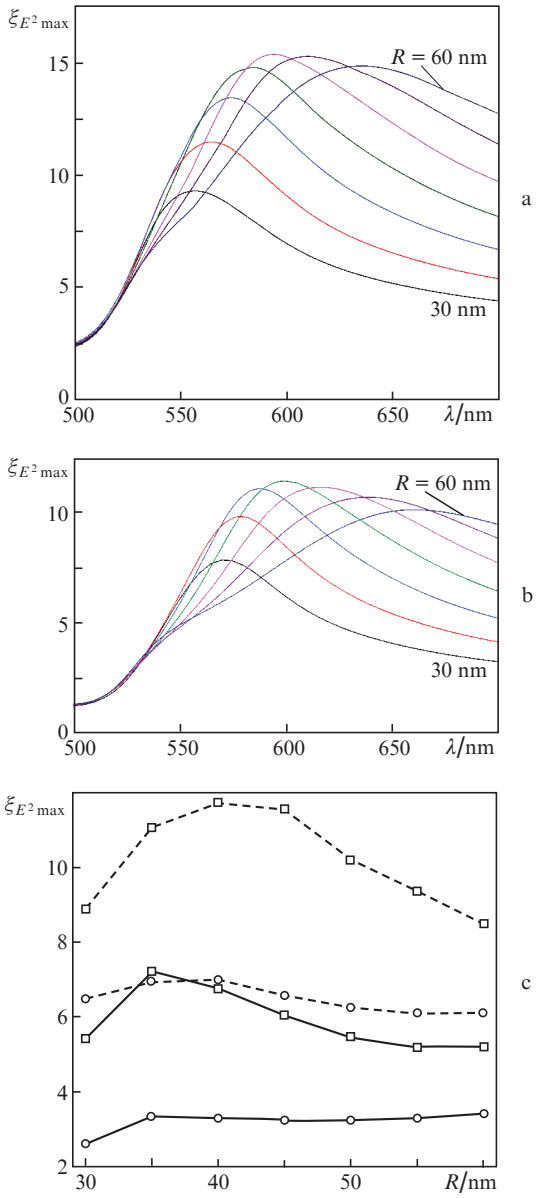

Figure 12. Spectral dependences of the maximum value of ξ_{E^2max} at a distance of 15 nm from the surface of nanospheres with different radii (the step in the radius of nanospheres corresponding to the neighboring curves is 5 nm) without coating (a) and with a protein coating (b), as well as the dependence of the enhancement factor ξ_{E^2max} on the radius of coated (solid curves) and uncoated (dashed curves) nanospheres at λ = 532 (circles) and 555 nm (squares) (c).

For comparison with the known experimental data [49], an additional numerical study of the plasmon properties of coated and uncoated nanospheres with diameters of 13 and 20 nm was performed. The simulation results are shown in Fig. 13. The calculations were carried out under the assumption that the shell thickness is directly proportional to the radius of the nanosphere; therefore, the distance in the radial direction from the sphere surface to the TagRFP layer is smaller for small nanospheres than for large ones. Thus, while

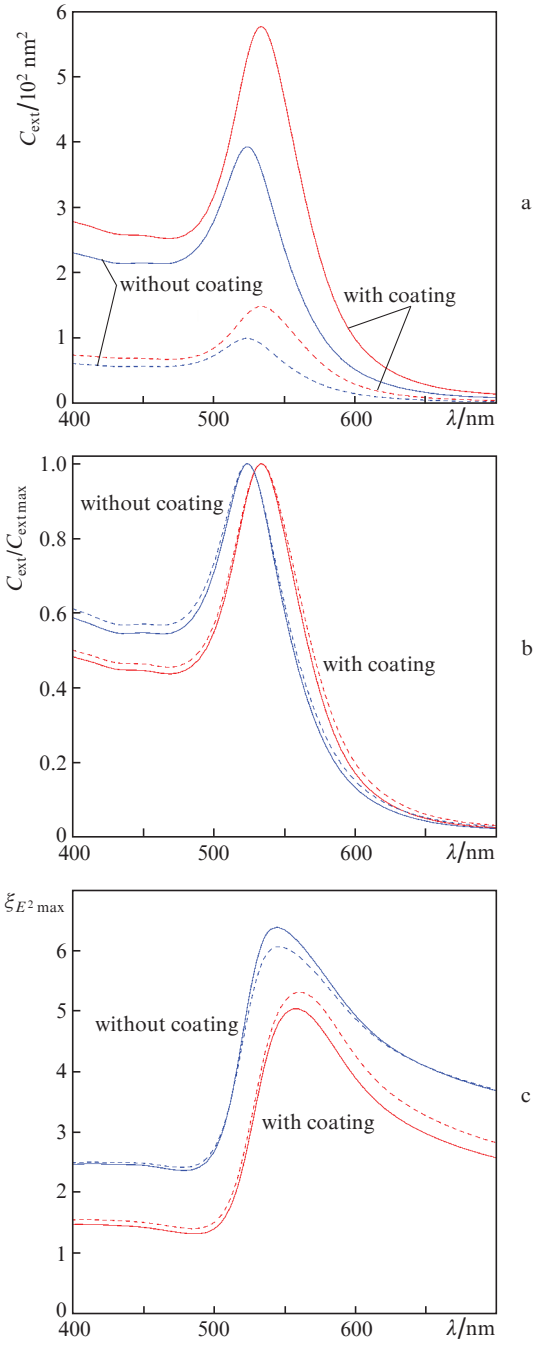

Figure 13. Spectral dependences of the extinction cross section (a), the normalised extinction cross section (b), and the maximum value of ξ_{E^2max} (c) in the region of the TagRFP fluorescent protein layer for nanospheres with a diameter of 20 nm (solid curves) and 13 nm (dashed curves).

for spheres with $R \geqslant 30$ nm the thickness of the sandwich shell was taken by us equal to 15 nm, for spheres with diameters of 13 and 20 nm it was 3 and 5 nm, respectively. This is in good agreement with the sizes of nanospheres and multilayer structures studied experimentally in [49]. It should be noted that the calculated normalised extinction spectra (Fig. 13b) are also in good agreement with the experimental results of studying the extinction of similar coated and uncoated nanospheres [49]. A comparison of the data obtained for spheres with a diameter of 60 nm (see Fig. 9c) and with diameters of 13 and 20 nm (Fig. 13), shows that, keeping in mind the coating thickness, they demonstrate rather close maximum values of ξ_{E^2} in the fluorescent protein attachment region, differing by no more than 40%. At the same time, nanoparticle-protein complexes based on small particles appear to be more promising for use in biomedical applications.

4. Conclusions

Mathematical models are constructed and numerical modelling of the near-field distribution within and in the vicinity of two types of GNPs (nanospheres and nanorods) intended for the manufacture of protein–GNP complexes and excitation of photosensitizers in the wavelength range of 532–770 nm is performed.

The features of the formation of zones of localisation of the optical field and the nature of the decrease in the corresponding enhancement factor ξ_{E^2} of the electric field strength of the laser beam with distance from the nanoparticles are investigated. The prospect of creating complexes based on gold nanorods with excitation of fluorescent proteins in the near-IR range, in which ξ_{E^2} is expected to increase by about 300 times as compared to complexes based on gold nanospheres is estimated.

The tendency of the red shift of the wavelength at which the maximum enhancement factor ξ_{E^2} of the local field is reached relative to the positions of the maxima of the absorption and scattering cross sections for uncoated gold nanospheres and multilayer structures is described. The influence of size effects on the localisation of fields in the studied protein structures is considered. A criterion for achieving a maximum of ξ_{E^2} in a structure with a multilayer coating is proposed to optimise the protein–GNP complexes and to increase the efficiency of laser radiation impact on fluorescent protein structures.

It is shown that nanospheres with a diameter of 13, 20, and 60 nm, taking into account the coating thickness, have close maximum local field enhancement factors ξ_{E^2}. At the same time, spheres of small diameter (13 and 20 nm) are preferable from the point of view of their permeability to the cell membrane. Achieving comparable ξ_{E^2} values for large and small spherical particles is an important result for the practical use of protein-GNP complexes in biomedical problems.

Acknowledgements. The work was supported by the Russian Foundation for Basic Research (Grant No. 19-54-06008 MNTI_a) and the Ministry of Science and Technology of Israel (Grant No. 3-16536). The results presented in Section 2 were obtained within the framework of the State Assignment of the Institute of Precision Mechanics and Control, Russian Academy of Sciences. The results shown in Fig. 4 were obtained under the support from the Russian Foundation for Basic Research (Grant No. 19-07-00378).

References

1. Vines J.B., Yoon J-H., Ryu N-E., Lim D.-J., Park H. *Front. Chem*., **7**, 167 (2019).
2. Dykman L., Khlebtsov N. *Gold Nanoparticles in Biomedical Applications* (Boca Raton–London–New York: CRC Press, 2017).
3. Maksimova I.L., Akchurin G.G., Terentyuk G.S., Khlebtsov B.N., Akchurin G.G. Jr., Ermolaev I.A., Skaptsov A.A., Revzina E.M., Tuchin V.V., Khlebtsov N.G. *Quantum Electron*., **38** (6), 536 (2008) [*Kvantovaya Elektron*., **38** (6), 536 (2008)].
4. Tuchina E.S., Tuchin V.V., Khlebtsov B.N., Khlebtsov N.G. *Quantum Electron*., **41** (4), 354 (2011) [*Kvantovaya Elektron*., **41** (4), 354 (2011)].
5. Genina E.A., Dolotov L.E., Bashkatov A.N., Terentyuk G.S., Maslyakova G.N., Zubkina E.A., Tuchin V.V., Yaroslavsky I.V., Altshuler G.B. *Quantum Electron*., **41** (5), 396 (2011) [*Kvantovaya Elektron*., **41** (5), 396 (2011)].
6. Genina E.A., Terentyuk G.S., Khlebtsov B.N., Bashkatov A.N., Tuchin V.V. *Quantum Electron*., **42** (6), 478 (2012) [*Kvantovaya Elektron*., **42** (6), 478 (2012)].
7. Tuchina E.S., Petrov P.O., Kozina K.V., Ratto F., Centi S., Pini R., Tuchin V.V. *Quantum Electron*., **44** (7), 683 (2014) [*Kvantovaya Elektron*., **44** (7), 683 (2014)].
8. Mieszawska A.J., Mulder W.J.M., Fayad Z.A., Cormode D.P. *Mol. Pharmaceutics*, **10** (3), 831 (2013).
9. Dobrovolskaia M.A., McNeil S.E. *Nat. Nanobiotechnol*., **2**, 469 (2007).
10. Duncan B., Kim C., Rotello V.M. *J. Controlled Release*, **148** (1), 122 (2010).
11. Bhattacharya R., Mukherjee P. *Adv. Drug Delivery Rev*., **60**, 1289 (2008).
12. Connor E.E., Mwamuka J., Gole A., Murphy C.J., Wyatt M.D. *Small*, **1** (3), 325 (2005).
13. Khlebtsov N.G., Dykman L.A. *Nanotechnologies in Russia*, **6** (1-2), 17 (2011) [*Ross. Nanotekh*., **6** (1-2), 39 (2011)].
14. Marchenkov N.S., Marchenko N.V. *Med. Fiz*., **4** (64), 64 (2014).
15. Motiei M., Dreifuss T., Betzer O., Panet H., Popovtzer A., Santana J., Abourbeh G., Mishani E., Popovtzer R. *ACS Nano*, **10**, 3469 (2016).
16. Dreifuss T., Betzer O., Shilo M., Popovtzer A., Motiei M., Popovtzer R. *Nanoscale*, **7**, 15175 (2015).
17. Betzer O., Ankri R., Motiei M., Popovtzer R. *J. Nanomater*., **2015**, 646713 (2015).
18. Eghtedari M., Liopo A.V., Copland J.A., Oraevsky A.A., Motamedi M. *Nano Lett*., **9**, 287 (2009).
19. Von Maltzahn G., Park J.H., Agrawal A., Bandaru N.K., Das S.K., Sailor M.J., Bhatia S.N. *Cancer Res*., **69** (9), 3892 (2009).
20. Jain P.K., Lee K.S., El-Sayed I.H., El-Sayed M.A. *J. Phys. Chem. B*, **110**, 7238 (2006).
21. Barnoy E.A., Popovtzer R., Fixler D. *J. Biophotonics*, **13** (9), e202000158 (2020).
22. Tregubov A.A., Nikitin P.I., Nikitin M.P. *Chem. Rev*., **118** (20), 10294 (2018).
23. Turkevich J., Stevenson P.C., Hillier J. *Discussion of the Faraday Society*, **11**, 55 (1951).
24. Zheng Y., MaY., Zeng J., Zhong X., Jin M., Li Z.-Y., Xia X. *Chem. Asian J*., **8** (4), 792 (2013).
25. Nikoobakht B., El-Sayed M.A. *Chem. Mater*., **15**, 1957 (2003).
26. Hermanson G.T., in *Bioconjugate Techniques* (Amsterdam–London–New York: Academic Press, 2013) pp 549–587.
27. Samokhvalov A.V., Safenkova I.V., Eremin S.A., Zherdev A.V., Dzantiev B.B. *Nanotechnologies in Russia*, **14** (7-8), 397 (2019) [*Ross. Nanotekh*., **14** (7-8), 91 (2019)].
28. Li S., Liu H., Hia Y., Deng Y., Zhang L., Lu Z., He N. *Theranostics*, **2** (10), 967 (2012).
29. Hao K., He Y., Lu H., Pu S., Zhang Y., Dong H., Zhang X. *Anal. Chim. Acta*, **954**, 114 (2017).
30. Olshinka A., Deam A.-E., Didkovski E., Weiss S., Ankri R., Goldenberg-Cohen N., Fixler D. *Materials*, **13** (2), 447 (2020).
31. Richtering W., Alberg I., Zentel R. *Small*, **16** (39), 2002162 (2020).
32. Liu J., Peng Q. *Acta Biomater*., **55**, 13 (2017).
33. Deliolanis N.C., Kasmieh R., Wurdinger T., Tannous B.A., Shah K., Ntziachristos V. *J. Biomed. Opt*., **13**, 044008 (2008).

34. Zlobovskaya O.A., Sarkisyan K.S., Lukyanov K.A. *Russ. J. Bioorg. Chem*., **41**, 266 (2015) [*Bioorgan. Khim*., **41**, 299 (2015)].
35. Celli J.P., Spring B.Q., Rizvi I., Evans C.L., Samkoe K.S., Verma S., Pogue B.W., Hasan T. *Chem. Rev*., **110**, 2795 (2010).
36. Prescott S.W., Mulvaney P. *J. Appl. Phys*., **99**, 123504 (2006).
37. Khlebtsov B.N., Khanadeev V.A., Burov A.M., Le Ru E.C., Khlebtsov N.G. *J. Phys. Chem. C*, **124** (19), 10647 (2020).
38. Johnson P.B., Christy R.W. *Phys. Rev. B*, **6**, 4370 (1972).
39. Khlebtsov N.G., Bogatyrev V.A., Dykman L.A., Melnikov A.G. *J. Colloid Interface Sci*., **180**, 436 (1996).
40. Khlebtsov N.G. *Quantum Electron*., **38**, 504 (2008) [*Kvantovaya Elektron*., **38**, 504 (2008)].
41. Foerster B., Joplin A., Kaefer K., Celiksoy S., Link S., Sönnichsen C. *ACS Nano*, **11**, 2886 (2017).
42. Coronado E.A., Schatz G.C. *J. Chem. Phys*., **119**, 3926 (2003).
43. Li Y., Zhang H. *J. Wuhan University Technology-Mater. Sci. Ed*., **30**, 1304 (2015).
44. Dreaden E.C., Austin L.A., Mackey M.A., El-Sayed M.A. *Ther. Delivery*, **3** (4), 457 (2012).
45. Spaas C., Dok R., Deschaume O., Roo B.D., Vervaele M., Seo J.W., Bartic C., Hoet P., van den Heuvel V., Nuyts S., Locquet J.-P. *Radiat. Res*., **185** (4), 384 (2016).
46. Nayhoz T., Barnoy E.A., Fixler D. *Materials*, **9** (11), 926 (2016).
47. https://www.fpbase.org/protein/tagrfp/.
48. Khlebtsov N.G., Dykman L.A., Bogatyrev V.A., Khlebtsov B.N. *Colloid J*., **65** (4), 508 (2003) [*Kolloidnyi Zh*., **65** (4), 552 (2003)].
49. Barnoy E.A., Motiei M., Tzror C., Rahimipour S., Popovtzer R., Fixler D. *ACS Appl. Nano Mater*., **2** (10), 6527 (2019).